Proton acceleration by collisionless shocks using a supersonic H 2 gas-jet target and high-power infrared laser pulses

P. Puyuelo-Valdes, J. Henares, F. Hannachi, T. Ceccotti, J. Domange, M. Ehret, E. d'Humieres, L. Lancia, Jean-Raphaël Marquès, X. Ribeyre, et al.

AUTHOR QUERY FORM

AIP Publishing	**Journal: Phys. Plasmas** **Article Number: POP19-AR-58116**	**Please provide your responses and any corrections by annotating this PDF and uploading it to AIP's eProof website as detailed in the Welcome email.**

Dear Author,

Below are the queries associated with your article; please answer all of these queries before sending the proof back to AIP.

Article checklist: In order to ensure greater accuracy, please check the following and make all necessary corrections before returning your proof.

1. Is the title of your article accurate and spelled correctly?
2. Please check affiliations including spelling, completeness, and correct linking to authors.
3. Did you remember to include acknowledgment of funding, if required, and is it accurate?

Location in article	Query / Remark: click on the Q link to navigate to the appropriate spot in the proof. There, insert your comments as a PDF annotation.
AQ1	Please check that the author names are in the proper order and spelled correctly. Also, please ensure that each author's given and surnames have been correctly identified (given names are highlighted in red and surnames appear in blue).
AQ2	Please define PSL at first occurrence.
AQ3	In Refs. 3–5, and 24 please provide a brief description of the information available at the website. For example, "See XX for information about XXX."
AQ4	Please check and confirm the edits made in Refs. 11 and 20.
AQ5	Please provide volume and page number for Ref. 12.
AQ6	Please specify which section or subsection "in the following section" refers to here.
AQ7	We were unable to locate a digital object identifier (doi) for Ref(s). 6, 7, 15, 21, 31. Please verify and correct author names and journal details (journal title, volume number, page number, and year) as needed and provide the doi. If a doi is not available, no other information is needed from you. For additional information on doi's, please select this link: http://www.doi.org/.
	Please confirm ORCIDs are accurate. If you wish to add an ORCID for any author that does not have one, you may do so now. For more information on ORCID, see https://orcid.org/. P. Puyuelo-Valdes- J. L. Henares - 0000-0001-8990-4839 F. Hannachi- T. Ceccotti- J. Domange- M. Ehret - 0000-0002-7671-6246

E. d'Humieres-
L. Lancia - 0000-0001-7501-3648
J.-R. Marquès-
X. Ribeyre - 0000-0002-9823-2744
J. J. Santos - 0000-0002-4737-8559
V. Tikhonchuk - 0000-0001-7532-5879
M. Tarisien - 0000-0002-6292-2241

Please check and confirm the Funder(s) and Grant Reference Number(s) provided with your submission:

Agence Nationale de la Recherche, Award/Contract Number 17-CE30-0026-~~02~~

Agence Nationale de la Recherche, Award/Contract Number 10-IDEX-03-02

Centre National de la Recherche Scientifique, Award/Contract Number ALP-IONS

Compute Canada, Award/Contract Number pve-323-ac

Conseil Régional Aquitaine, Award/Contract Number POPRA

Please add any additional funding sources not stated above:

Thank you for your assistance.

Physics of Plasmas ARTICLE scitation.org/journal/php

Proton acceleration by collisionless shocks using a supersonic H_2 gas-jet target and high-power infrared laser pulses

Cite as: Phys. Plasmas **26**, 000000 (2019); doi: 10.1063/1.5116337
Submitted: 25 June 2019 · Accepted: 22 November 2019 ·
Published Online: 0 Month 0000

View Online Export Citation CrossMark

AQ1 P. Puyuelo-Valdes,[1,2] J. L. Henares,[1] F. Hannachi,[1] T. Ceccotti,[3] J. Domange,[1] M. Ehret,[4,5] E. d'Humieres,[4] L. Lancia,[6] J.-R. Marquès,[6] X. Ribeyre,[4] J. J. Santos,[4] V. Tikhonchuk,[4] and M. Tarisien[1]

AFFILIATIONS

[1]CENBG, CNRS-IN2P3, Université de Bordeaux, 33175 Gradignan Cedex, France
[2]INRS-EMT, 1650 blvd. Lionel-Boulet, Varennes, Quebec J3X 1P7, Canada
[3]LIDYL, CNRS, CEA, Université de Paris-Saclay, 91191 Gif-Sur-Yvette Cedex, France
[4]CELIA, CNRS, CEA, Université de Bordeaux, UMR 5107, 33400 Talence, France
[5]Institut für Kernphysik, Technische Universität Darmstadt, 64289 Darmstadt, Germany
[6]LULI, Ecole Polytechnique, 91128 Palaiseau Cedex, France

ABSTRACT

For most laser-driven ion acceleration applications, a well-characterized intense ion beam with a low divergence and a controllable energy spectrum produced at a high repetition rate is needed. Gas-jet targets have given promising results in simulations, and they have several technical advantages for high-repetition-rate lasers. In this work, we report on proton acceleration to energies up to 6 MeV using a supersonic H_2 gas-jet target at the LULI PICO2000 laser facility. The experimental results are compared with the plasma hydrodynamics and the particle-in-cell simulations to identify the acceleration mechanisms at play.

I. INTRODUCTION

Laser-driven ion acceleration techniques are under rapid development due to a large potential range of applications.[1,2] For most of them, a well-characterized intense ion beam with a well-defined energy distribution is needed. This requires the quantitative optimization of the laser-matter interaction parameters. Numerical simulations help to identify the most appropriate parameters related to the explored acceleration mechanism. Nevertheless, the experimental phase of such an optimization work is quite time consuming. Now, with the new generation of high-power laser facilities operating at a high repetition rate (as APOLLON in France,[3] ELI pillars in Europe,[4] or VEGA in Spain[5]), this is more accessible.

Solid targets are used for ion acceleration in most experiments for their high density, the simplicity of fabrication, and alignment. However, the replacement and the realignment of the target are mandatory after each laser shot, and the interaction generates debris that damages the optical elements. A large effort has been made to develop fast-moving, high-repetition-rate target holders which contain several solid targets. Even if considerable improvement has been achieved, avoiding debris deposition and target replacement after several shots still represent a challenge. A particular kind of solid target, which can be regenerated *in situ*, is cryogenic ribbons.[6,7] These could be clean sources of protons or deuterons, free of contaminants and operating at a high repetition rate. For instance, a flux of 10^9 protons/MeV/sr with a maximum energy of 18 MeV was reported at the 150 TW ultrashort pulse laser Draco, HZDR with a planar $(20 \times 2\,\mu m^2)$ cryogenic hydrogen jet.[7] The acceleration regime was Target Normal Sheath Acceleration (TNSA) producing broad energy distributions.[8]

Another option consists of using liquid targets as water droplets[9–12] or liquid crystal films.[13] In 2018, Hilz *et al.*[12] observed proton bunches with energies between 20 and 40 MeV using the PHELIX PW laser at GSI delivering 500 fs pulses with an energy of 150 J. The acceleration mechanism reported is the Coulomb repulsion.

Near-critical-density gas-jet targets are an interesting alternative for the acceleration of different ion species as they can be used at a high repetition rate and are debris-free. Moreover, a strong electrostatic field inducing a more efficient ion acceleration than TNSA can be produced in near-critical-density plasmas. This acceleration scheme involving collisionless shock waves had been first introduced by Silva *et al.*[14] for overdense plasma targets and expanded by d'Humières

Physics of Plasmas ARTICLE scitation.org/journal/php

et al.[15] to underdense ones. In near-critical-density plasmas using a CO_2 laser, Haberberger *et al.*[16] demonstrated that the laser-driven collisionless shocks can accelerate proton beams to 20 MeV with a narrow energy spread of about 1% and a low emittance.

Gas jets are promising targets, and nozzles capable of generating the required plasma densities have to be designed. Several results were published using CO_2 lasers, which correspond to a critical density (n_c) of $10^{19}\,\text{cm}^{-3}$.[16–18] However, the presently developed high-energy near-infrared lasers correspond to $n_c \sim 10^{21}\,\text{cm}^{-3}$, which are still very challenging to produce with supersonic gas jets. Only a few experiments have been performed so far. In 2013, Sylla *et al.*[19] carried out one with the "Salle Jaune" laser at LOA using a submillimetric supersonic 0.95 n_c density helium jet from a conical nozzle. They observed He^+ ions with energies of up to 250 keV in the transverse direction. In 2017, Chen *et al.*[20] at the TITAN laser facility at LLNL used a supersonic 2.5 n_c density hydrogen jet from a rectangular nozzle and observed protons with energies of up to 0.8 MeV in the longitudinal direction.

We have developed a series of near-critical gas-jet targets for 1 μm wavelength lasers. Computational fluid dynamics (CFD) simulations have been performed to design the corresponding supersonic gas-jet nozzles. The target density profiles were measured by interferometry and compared with the simulation results. More details have been published in Refs. 21 and 22.

In this paper, we report on the proton acceleration of up to 6 MeV in a high-density H_2 gas jet at the PICO2000 laser facility at LULI. Hereinafter, the setup and the experimental results are presented. The latter are compared with the hydrodynamics and the Particle-in-Cell (PIC) simulations.

II. EXPERIMENTAL SETUP

A 1000 bar Haskel gas booster coupled to a Clark-Cooper solenoid valve and a convergent-divergent conical nozzle (a 100 μm throat diameter, a 1 mm length, and a 240 μm exit diameter) were employed to generate supersonic H_2 gas-jet targets. The PICO2000 laser beam at a wavelength $\lambda = 1053$ nm, a 1 ps pulse duration, and a 60 J energy was focused on the gas jet, at 400 μm from the nozzle exit, in a 12 μm Full Width at Half Maximum (FWHM) diameter spot providing an intensity of 5×10^{19} W/cm^2. The Amplified Spontaneous Emission (ASE) duration was of the order of 250 ps, with its level $\sim 10^6$ below the picosecond pulse maximum.

The gas-jet target alignment was achieved using the bottom and the side views placed in the chamber. Four Thomson Parabolas (TP) with their respective Imaging Plate detectors (IP) were used to detect and resolve the accelerated ions in charge and energy. They were placed at 0°, 30°, 70°, and 80° with respect to the laser axis (Fig. 1). They were shielded by lead walls for a signal-to-background ratio improvement and were equipped with pinholes at their entrances for a better energy resolution. BAS-TR and BAS-MS IPs from the Fuji Photo-Film Co. Ltd., were used and analyzed using a FUJIFILM FLA-700 reader. The IP response function to protons has been taken from Ref. 23. All TPs have been calibrated in energy at the AIFIRA accelerator facility at CENBG,[24] in the energy range from 500 keV to 3.5 MeV. The uncertainties in the energy value and in the number of protons/MeV/sr (N_p/MeV/sr) were calculated assuming that all variables (solid angle, response function, number of PSL, energy calibration) are statistically independent and summing their variances. The energy is measured with an accuracy of about 3%. The accuracy of N_p/MeV/sr is about 50% at low energies and about 20% at high energies.

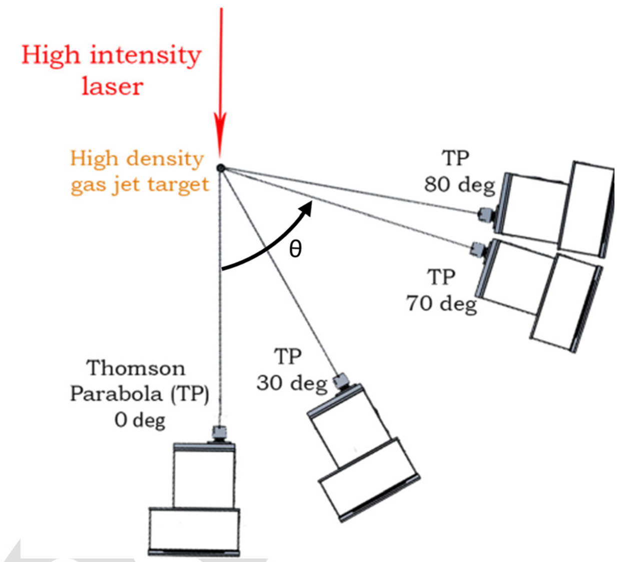

FIG. 1. Experimental setup at the LULI facility: PICO2000 high-power laser was incident on a high-density H_2 gas jet. Four Thomson Parabolas (TPs) equipped with Imaging Plate detectors (IPs) were placed at 0°, 30°, 70°, and 80° with respect to the laser axis.

The BAS-MS films have a 9 μm protective layer which stops protons with energies lower than 600 keV, while the BAS-TR films are layer-free. Examples of the proton spectra in Fig. 2 show about a one order of magnitude difference in their background levels. The BAS-TR IPs display a background of $(1.9 \times 10^9 \pm 1.4 \times 10^9)$ protons/MeV/sr, while for the BAS-MS IPs, it is $(0.25 \times 10^9 \pm 0.22 \times 10^9)$ protons/MeV/sr. This is probably due to their different sensibility to UV light. Therefore, we chose to employ the BAS-MS IPs despite the loss of the lowest part of the energy distribution.

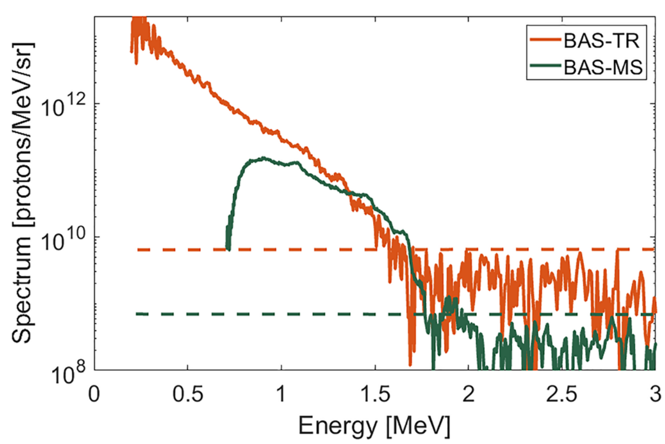

FIG. 2. Proton energy spectra recorded at 30° from two analog shots using both types of IPs. The one in orange is from a BAS-TR IP, while the green one is from the BAS-MS IP. Dashed lines indicate the detection limit corresponding to the mean value of the background level plus two times its variance.

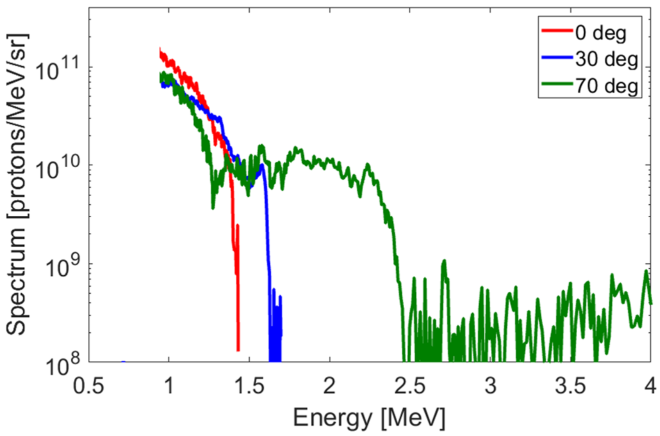

FIG. 3. Proton energy spectra at 0° (red), 30° (blue), and 70° (green) obtained with the laser focused at the center of the jet.

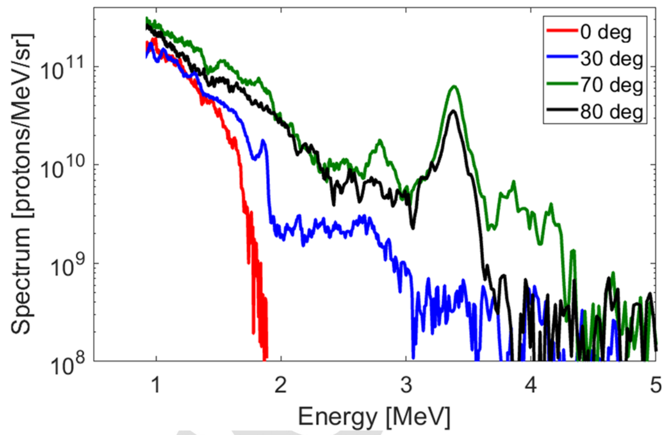

FIG. 5. Proton energy spectra at 0° (red), 30° (blue), 70° (green), and 80° (black) obtained with the laser focused at the rising slope of the jet density profile.

III. EXPERIMENTAL RESULTS

Figure 3 shows the typical spectra obtained with the laser focused at the center of the gas jet. About 10^{11} protons/MeV/sr in a continuous energy distribution of up to 1.5 MeV are observed in the longitudinal direction (0°). A similar flux in that same energy range is also observed in the other directions (30° and 70°). Furthermore, a second structure of up to 2.5 MeV is observed in the transverse direction containing 10^{10} protons/MeV/sr. Unfortunately, the TP at 80° was not in place on these first shots.

The proton maximum energy was increased when the laser was focused at the rising slope of the gas-jet density profile, at about 70 μm from its center. Figure 4 shows the typical spectra recorded in this configuration. Besides the structures already presented in Fig. 3, an additional peak at 2.3 MeV is observed at 0°. A high proton flux (about 10^{11} protons/MeV/sr) in the energy range of up to 3 MeV is also observed in the transverse direction.

It is worth noting that the angular position and the energy of the peaked structure at 0° in Fig. 4 are highly dependent on the laser and the target parameters. Small variations of these (for example, lower maximum density of the gas jet and laser fluctuations) can shift the peak to the transverse directions (70° and 80°) and to higher energies (3.3 MeV), as seen in Fig. 5. In addition, a plateau structure in the energy range of 2–3 MeV is observed at 30°. Similar features in the transverse direction can be seen in Figs. 3 and 4.

The effect of ASE on the proton spectra was also studied. The level of ASE is controlled by the variation of the timing of two Pockels cells which isolate the main short picosecond pulse from the amplified nanosecond background. Figure 6 presents the proton energy distribution when the ASE level is reduced at the minimum achievable. The spectra display more complex structures. The proton flux at 80° is smaller than in previous shots, while the maximum energy at 0° is higher. Three particular features can be seen on the spectrum in the longitudinal direction. The proton flux drops from 10^{11} to 10^{9} in the energy range between 0.5 and 2 MeV. Then, it increases up to 10^{10} between 1.7 and 3 MeV, and a third peak with a flux of 5×10^{9} is

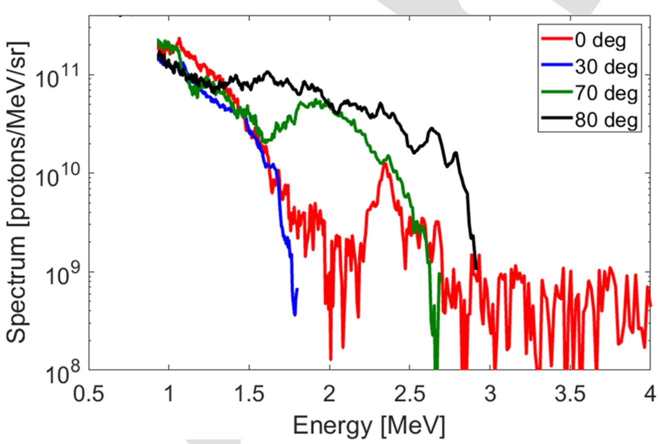

FIG. 4. Proton energy spectra at 0° (red), 30° (blue), 70° (green), and 80° (black) obtained with the laser focused at the rising slope of the jet density profile.

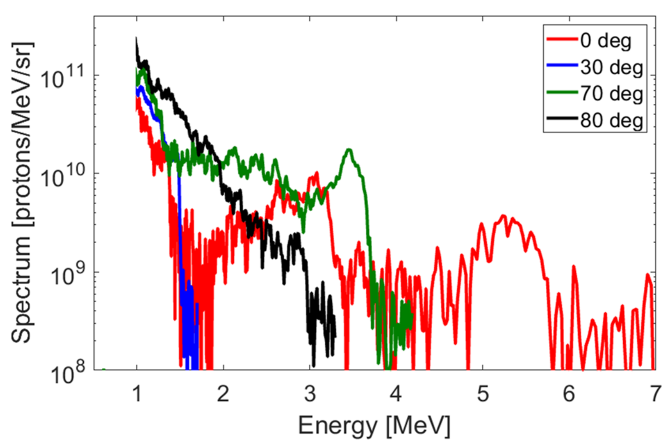

FIG. 6. Proton energy spectra at 0° (red), 30° (blue), 70° (green), and 80° (black) obtained with the laser focused at the rising slope of the jet density profile. The ASE level was reduced for this shot.

Physics of Plasmas ARTICLE scitation.org/journal/php

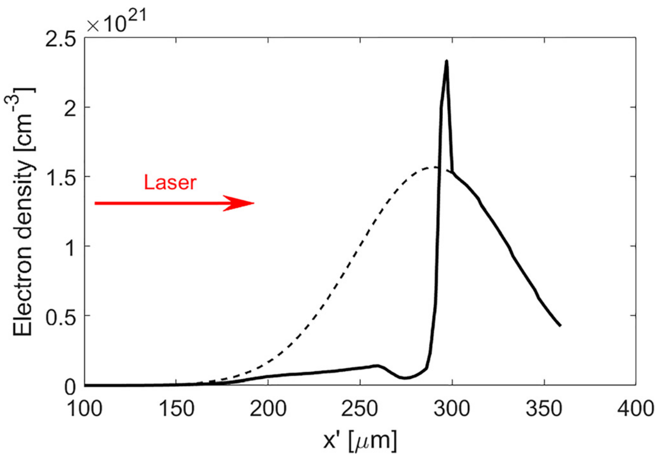

FIG. 7. Dashed line: the initial density profile of the gas jet based on measurements. Solid line: the density profile calculated with the FLASH code taking into account the laser ASE and used as input in the PIC simulations.

observed in the range of 4.3–5.3 MeV. Another peak at the energy of 3.4 MeV can also be seen at 70°.

IV. HYDRODYNAMICS AND PIC SIMULATIONS

Numerical simulations with the two-dimensional Particle-in-Cell (2D PIC) code, PICLS,[25] were used for the interpretation of the measured proton spectra. The PICO2000 laser parameters at the normal incidence and the s-polarization were used as inputs. The temporal and the spatial laser intensity profiles are described by the truncated Gaussian functions. The laser temporal pulse is truncated at 2 ps. The pulse is injected at the left side of the simulation box ($600 \times 160\ \mu m^2$) at a time $t = 0$. Assuming that the high-intensity laser pulse fully ionizes the gas, the target is described as a 380 μm length plasma of electrons and protons. The mesh size is 80 nm, and 15 particles of each species were used in each cell. Physical processes are simulated during 3.6 ps with a time step of 0.267 fs. Absorbing boundary conditions for the fields and the particles are applied.

The plasma density profile in the PIC simulations accounts for the interaction of the laser ASE with the initial gas density profile. This has been modeled with the 3D hydrodynamic code FLASH.[26] In this simulation, the gas jet is contained in a cylinder of a 200 μm diameter center on the maximum of its radial density profile. The dimensions of the simulation box are $560 \times 120 \times 120\ \mu m^3$, and the center of the cylinder is at $x' = 290\ \mu m$ from the laser arrival side. The prepulse radial distribution is the same as the main pulse one with the maximum intensity reduced by a factor of 10^6 (corresponding to the cut of 1 ns on the Pockels cell timing).

For example, Fig. 7 shows the initial Gaussian density profile of the gas jet (dashed line) and the calculated density profile (solid line) in the laser propagation direction 240 ps after the start of the simulation, which is of the order of the ASE duration in the experiment. The left part of the initial density profile is dramatically modified, and a shock is formed with a peak of approximately twice the original density. The exact location of the peak and its magnitude depend on the ASE duration which has not been precisely measured in this experiment. The consequences of a different density profile are discussed at the end of Sec. IV. A low-density plasma remains in the left part of the density profile.

In Fig. 8, a 2D slice of the 3D electron density calculated with the code FLASH at $t = 240$ ps is represented. It shows that the laser penetrates up to the critical density and produces a density channel in the gas jet. It is worth noting that the density on the y axis is constant over the focal spot diameter of 12 μm; therefore a constant y density is introduced in the PIC simulations.

The plasma density profile used as input in the PIC simulations is shown in Fig. 9(1). To simplify the calculations, the plasma density on the x axis is assumed to be constant ($\sim 10^{19}\ cm^{-3}$) for $x < 185\ \mu m$ and increases to the maximum value of $\sim 2.4 \times 10^{21}\ cm^{-3}$ over a

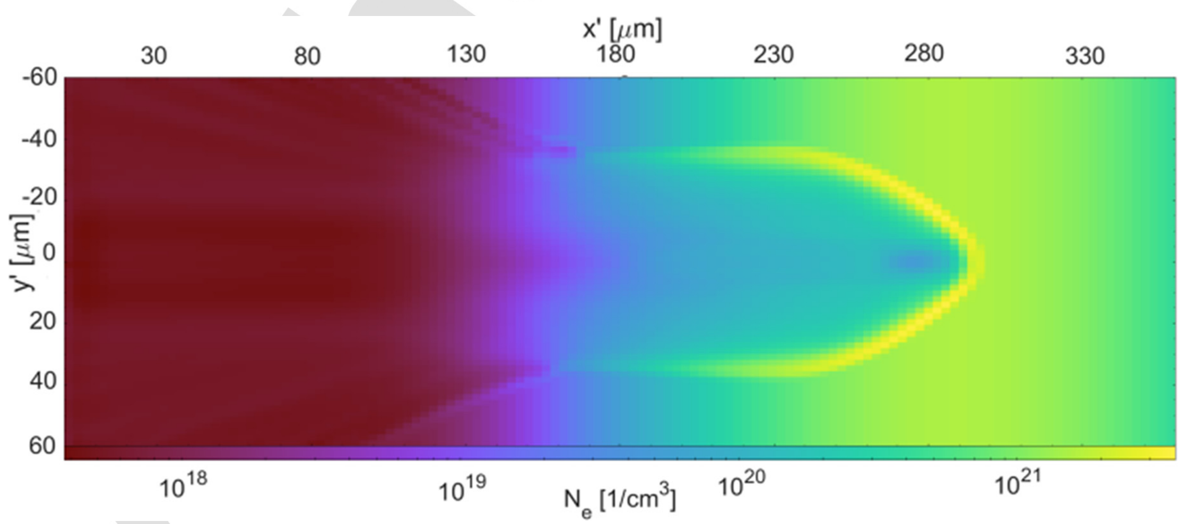

FIG. 8. 2D slice of the 3D electron density in the FLASH simulation at $t = 240$ ps, the time of the main pulse arrival.

J_ID: PHPAEN DOI: 10.1063/1.5116337 Date: 7-December-19 Stage: Page: 5 Total Pages: 12

PROOF COPY [POP19-AR-58116]

distance of 5 μm, ($x = 190$ μm in the PIC simulation corresponds to $x' = 297$ μm in FLASH simulations since the left edge of the plasma was defined as $x = 0$ in the PIC simulations). For $x > 200$ μm, the initial Gaussian profile has been used without any modification. Sharp plasma borders generate artifacts in the PIC simulation. Since real gas edges are not sharp, a slope of 15% of the plasma length was used at each border of the plasma in order to minimize this effect. Particles accelerated in these parts are not considered in the analysis. The initial plasma temperature is set to zero.

The PIC simulation results are presented in Fig. 9 for the particle energy density at four consecutive instants and are discussed in detail in the following sections: AQ6

- $t = 1$ ps, laser penetrates to the density of $\sim 10^{19}$ cm^{-3} [Fig. 9(a), Sec. IV A];
- $t = 1.8$ ps, laser attains the maximum plasma density of $> n_c$ [Fig. 9(b), Sec. IV B];
- $t = 2.3$ ps, soon after [Fig. 9(c), Sec. IV B]; and
- $t = 3.6$ ps, at the end of the simulation [Fig. 9(d), Sec. IV C].

A. Laser interaction with the underdense plasma

As the laser penetrates in the underdense plasma, the electrons are heated and expelled radially by the laser ponderomotive force. A channel is formed, and the protons are accelerated radially by the charge separation electric field. At $t = 1$ ps, self-focusing and self-channeling of the laser pulse are observed. These are due to the electron expulsion by the laser ponderomotive force and the relativistic increase in the electron mass. As the laser pulse power is larger than the critical power of self-focusing, multiple filaments are formed [Fig. 9(a)].

The proton phase spaces at $t = 1$ ps are shown in Fig. 10. At first, the protons are accelerated at the plasma edge $x = 0$. However, the radial acceleration dominates: the transverse momentum, p_y, displayed in Fig. 10(b) is much larger than the longitudinal one, p_x, shown in Fig. 10(a).

The proton angular energy distribution in the forward ($p_x \geq 0$) direction is displayed in Fig. 11. Most of the protons are accelerated in the transverse direction during the laser channeling in the underdense

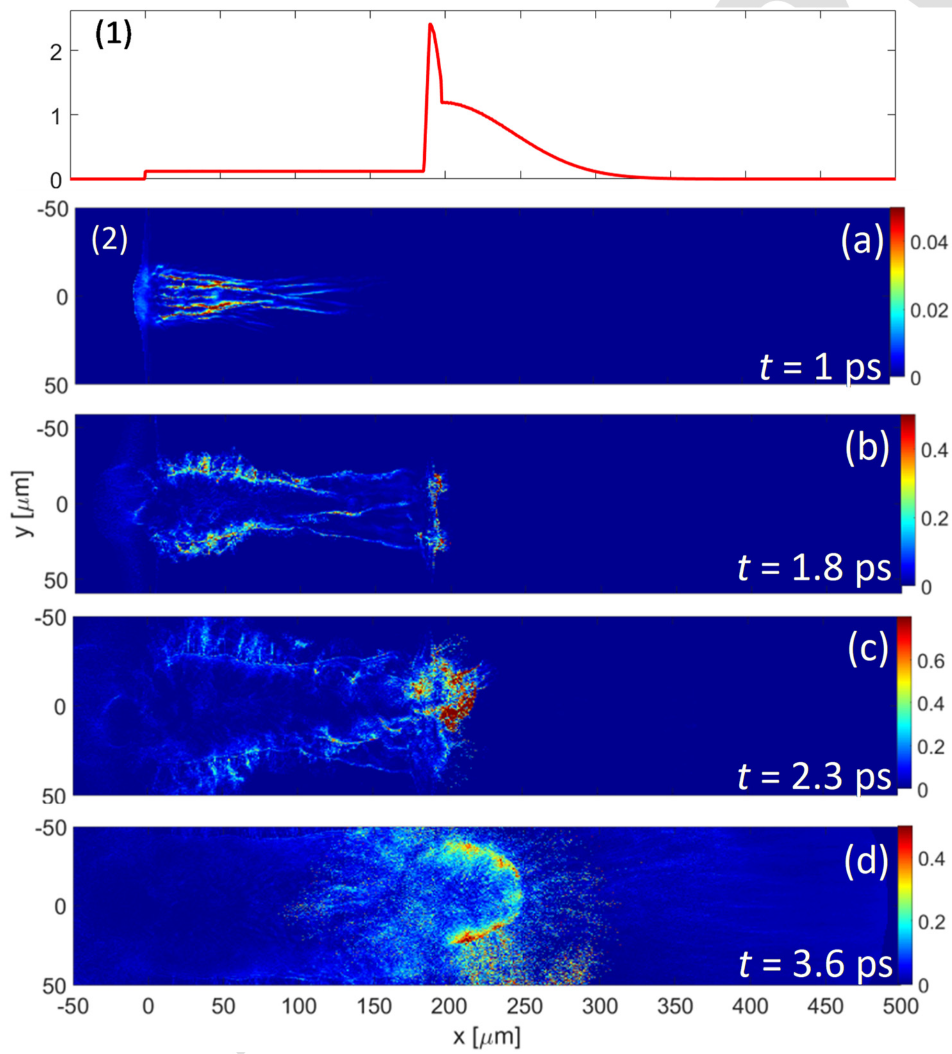

FIG. 9. (1) Proton density profile (in n_c units) at $t = 0$ ps. (2) Evolution of the proton energy density (in relativistic units, $n_c m_e c2$) in the PIC simulation: (a) $t = 1$ ps, (b) 1.8 ps, (c) 2.3 ps, and (d) 3.6 ps.

ID: aipepub3b2server Time: 08:02 I Path: D:/AIP/Support/XML_Signal_Tmp/AI-PHP#190920

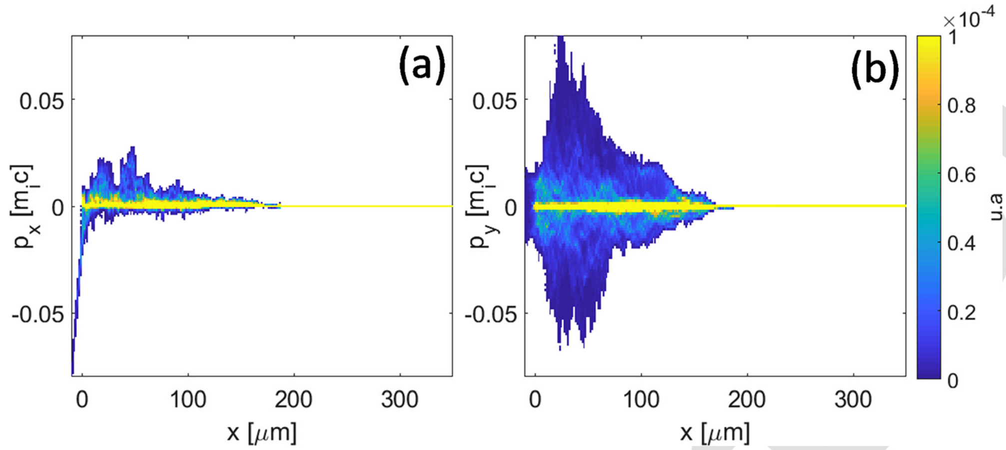

FIG. 10. Proton phase space histogram at time $t = 1$ ps: (a) longitudinal and (b) transverse momenta as a function of the longitudinal coordinate.

plasma. This particular feature of gas-jet experiments has been reported even in the case of helium acceleration.[19,27–31]

B. Laser interaction with the overcritical plasma

At $t = 1.8$ ps when the laser pulse reaches the maximum target density, one observes more complex interaction processes. Figure 12(a) evidence a collisionless shock formed at $x = 185\,\mu$m which accelerates protons both forward and backward (see the red box). This shock is the result of the laser intensity profile steepening: the increased radiation pressure pushes the plasma density forward, and the so-called hole boring process takes place [Fig. 9(b)].[32] The proton acceleration in the shock is essentially longitudinal. However, there is a small component in the transverse direction as shown in Fig. 12(b).

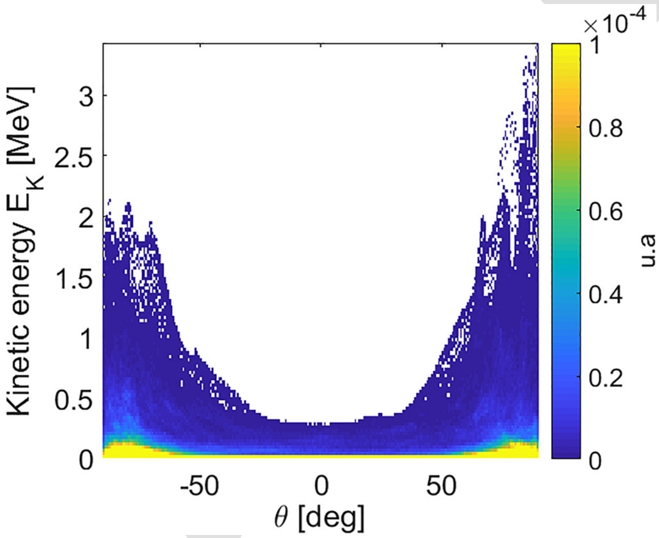

FIG. 11. Angular energy distribution of forward ($p_x \geq 0$) accelerated protons at $t = 1$ ps.

The angular energy distribution of protons accelerated in the forward direction is presented in Fig. 13(a). Similarly to the previous instant shown in Fig. 11, the majority of protons are accelerated in the transverse direction. However, there is a small fraction of protons that are accelerated in the longitudinal direction. Figure 13(b) confirms their origin: the angular energy distribution of the protons accelerated in the interval $x = 185\,\mu$m and $x = 210\,\mu$m presents a forward energetic component as shown in the phase space in the red square in Fig. 12.

In the hole boring process, the details of the shock instability strongly depend on the interaction conditions: the initial plasma temperature and the density profile.[33] Figure 14(b) shows the shock-accelerated protons in the direction of 50° with energies of up to 25 MeV higher than those accelerated by laser channeling (up to 15 MeV). Furthermore, in Fig. 15, which represents the spatial distribution of the period-averaged electromagnetic laser energy at $t = 2.3$ ps, one can see that most part of the laser is reflected at $x = 185\,\mu$m, except for a small part in which the direction is also bent.

C. Longer times: Laser beam collapse

The laser beam, which has deviated from its initial propagation direction, cannot penetrate further in the plasma. For $t > 2.5$ ps in the simulation [Fig. 9(d)], we observe the laser beam collapse as previously reported in Ref. 19.

Figure 16 shows the simulated proton energy distribution in the directions where TPs were set in the experiment within 10° wide angular windows. The spectra at all angles are continuously decreasing, while at the angles of 0° and 30°, there is a second plateau structure at a high energy. The latter is due to the particles accelerated by the collisionless shock, already analyzed in Sec. IV B and observed in Fig. 14.

D. Discussion

The goal of these simulations was to interpret the measured proton spectra and understand their origins. Figure 16 allows to compare the simulated energy distributions with the measured ones (Sec. III). However, it is worth noting that the maximum energies and the higher particle fluxes are found at 50° in the simulation (Fig. 14).

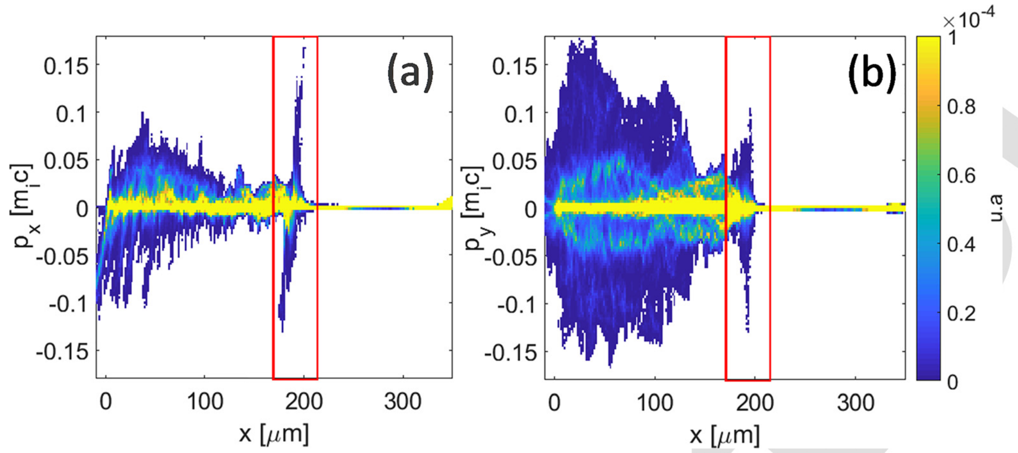

FIG. 12. Proton phase space histogram at time $t = 1.8$ ps: (a) longitudinal and (b) transverse momenta as a function of the longitudinal coordinate.

Isotropic acceleration with an average flux of 10^{11} protons/MeV/sr in the energy range of up to 1.5 MeV, observed in the experiment, is well reproduced in the PIC simulation. The energy range is higher than in the experiment, which can be explained by the fact that proton energies can be overestimated in 2D simulations.[34] This broad angle acceleration is present because the laser interacts first with a smooth plasma density profile. Its maximum energy depends on the length of the laser path before collapse.

We also succeeded to identify the collisionless shock produced in the hole boring process as the origin of the plateau in the proton energy distribution at near forward directions. The energy range of the plateau and the direction of the proton propagation depend on the initial conditions: the characteristics of the laser pulse and the ASE level. It was observed that the initial shock direction was the longitudinal one. However, the deviation of the laser beam affects the angular distribution of the energy plateau at longer times. In particular, it is influenced by the laser self-focusing in the underdense plasma. The subsequent filaments of the laser beam interact separately with the steepest part of the density profile producing their deflection. In the experiment, the laser interacts with the gas before $x = 0$ due to the smooth border of the gas profile. This means that the laser may not, in fact, focus at the simulated focal point and the curvature of its trajectory can be different from the simulated one. It is highly probable that the laser beam bends to higher angles inducing a plateau structure in the transverse direction as seen in the experiment. Concerning the ASE level, the worst contrast may generate a less steep density slope at $x = 185$ μm, leading to smaller plateau structures.

A striking feature of the experimental energy spectra is the peaked structures. They are measured at different angles depending on the laser shot. In the simulation spectrum shown in Fig. 17, a high-energy particle bunch separated from the principal structure is also observed at 12 MeV in the 23° direction. These types of features are highly dependent on the initial parameters of the simulation and, in this case, are not predicted at the angles where the parabolas were placed in the experiment.

V. CONCLUSION

In our experiment, proton acceleration is observed at 0°, 30°, 70°, and 80° using a supersonic H_2 gas-jet target. An isotropic

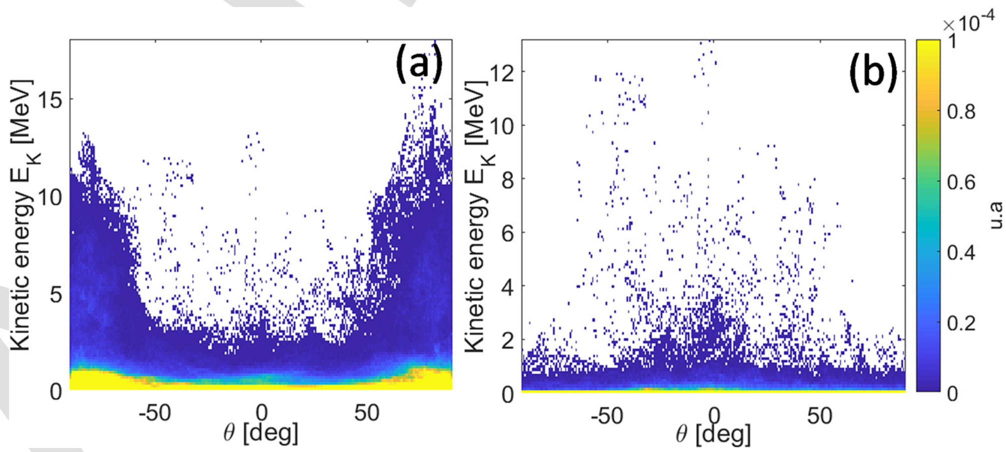

FIG. 13. Angular energy distribution of (a) all forward-accelerated protons and (b) forward protons accelerated between $x = 185$ μm and $x = 210$ μm at $t = 1.8$ ps.

Physics of Plasmas ARTICLE scitation.org/journal/php

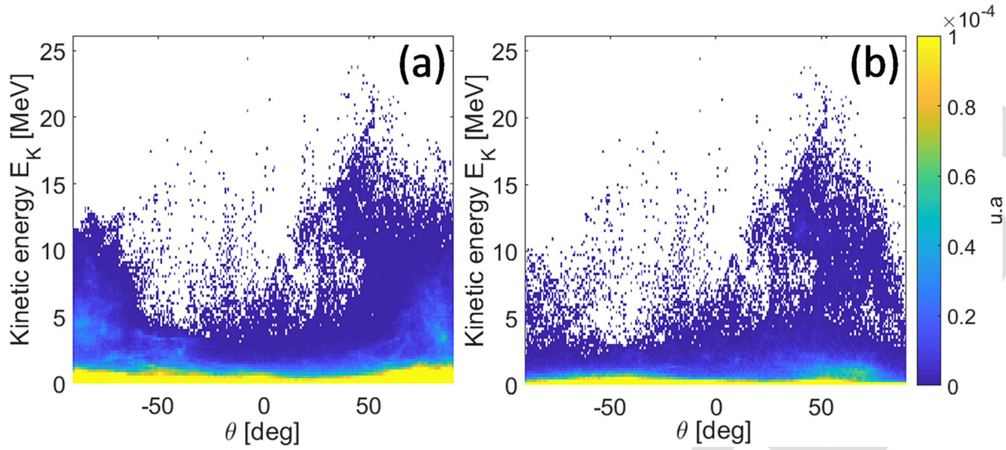

FIG. 14. Angular energy distribution of (a) all forward-accelerated protons and (b) forward shock protons accelerated in the interval $x = 185\ \mu$m to $x = 250\ \mu$m at $t = 2.3$ ps.

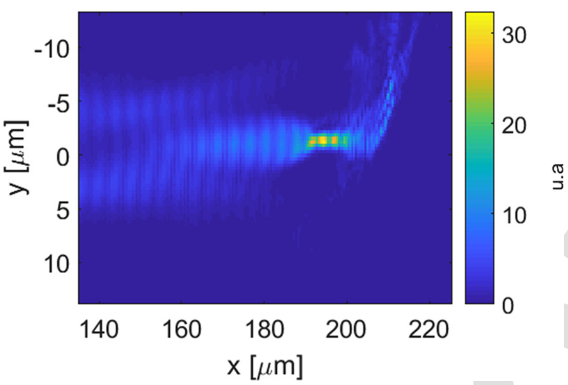

FIG. 15. Period-averaged electromagnetic laser energy $Ez^2 + Ey^2 + (cBz)^2$ at 2.3 ps.

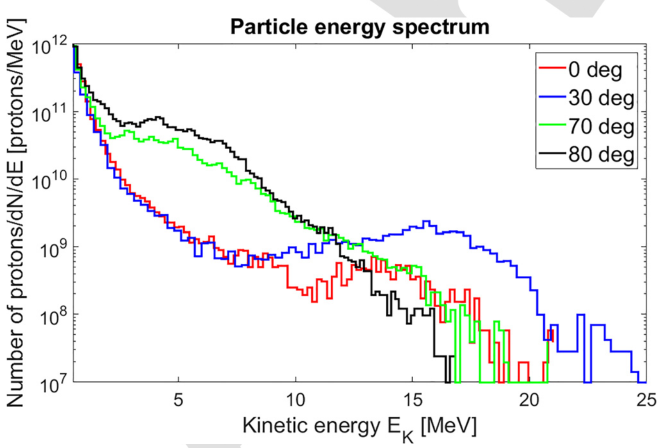

FIG. 16. Forward proton energy distribution at 3.6 ps from the PIC simulations. A 10° wide angular window was taken for each spectrum.

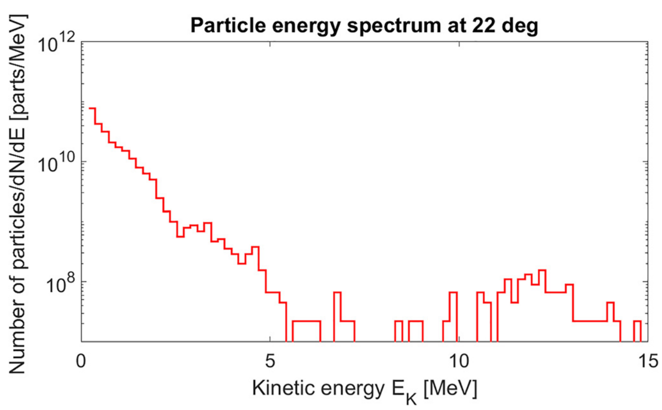

FIG. 17. Forward proton energy distribution at 3.6 ps from the PIC simulations from 21° to 23°.

acceleration with a flux of 10^{11} protons/MeV/sr is measured at low energies of up to 1.5 MeV. Furthermore, a second structure with a constant flux of particles (plateau) is observed in the transverse directions, sometimes even at 30° (Fig. 5). During the experiment, we have verified the advantage of focusing the laser at the rising slope of the gas density profile and of the use of a cleaner pulse by reducing the ASE level. In the best conditions, a maximum energy of 6 MeV was observed in the longitudinal direction. Energy spectra were successfully explained using plasma hydrodynamics and the PIC simulation codes. Self-focusing and self-channeling of the laser beam were observed in the underdense part of the plasma. It is responsible for the transverse acceleration reported. Moreover, a dramatic change of the density profile, produced by the reduction of the ASE level, induces a collisionless shock during the hole boring process. This shock accelerates protons to higher energies creating plateau structures in the spectra. Energetic peaked structures are observed at different angles in several shots which were also found in the simulations.

To our knowledge, these are the first significant high-energy proton spectra from the proton acceleration experiments when high-power infrared lasers interact with the supersonic gas-jet targets. As

Physics of Plasmas ARTICLE scitation.org/journal/php

explained above, a less than 1 MeV proton energy was reported in Refs. 19 and 20.

In the future, we want to improve the gas-jet density profile in order to enhance the collisionless shock acceleration in the longitudinal direction with respect to other processes. This will be achieved by designing new nozzles and adding optical shaping of the plasma target.[35]

ACKNOWLEDGMENTS

The authors would like to thank the staff of the LULI facility and the CENBG technical departments for the technical assistance during the experiment, in particular, Edouard Veuillot for his permanent help, Mathieu Chevrot for his outstanding involvement during the experiment, Simon Vallières for his help with the PIC simulations, and Laurent Gremillet for enlightening discussions. This work is supported by Nos. ANR-17-CE30-0026-02, POPRA, and IN2P3-CNRS 2016-2020 (ALP-IONS projects) grants; M.E. and J.J.S. acknowledge the financial support from the Programme IdEx Bordeaux—LAPHIA (No. ANR-10-IDEX-03-02). PIC simulations are possible with the use of High Performance Computing resources of Compute Canada (Job: pve-323-ac, P. Antici). The FLASH software used was developed, in part, by the DOE NNSA ASC- and the DOE Office of Science ASCR-supported Flash Center for Computational Science at the University of Chicago.

REFERENCES

[1]H. Daido, M. Nishiuchi, and A. S. Pirozhkov, "Review of laser-driven ion sources and their applications," Rep. Prog. Phys. 75, 056401 (2012).
[2]L. Pommarel, B. Vauzour, F. Mégnin-Chanet, E. Bayart, O. Delmas, F. Goudjil, C. Nauraye, V. Letellier, F. Pouzoulet, F. Schillaci, F. Romano, V. Scuderi, G. A. P. Cirrone, E. Deutsch, A. Flacco, and V. Malka, "Spectral and spatial shaping of a laser-produced ion beam for radiation-biology experiments," Phys. Rev. Accel. Beams 20, 032801 (2017).
AQ3 [3]See http://www.apollon-laser.fr/ for ■.
[4]See https://eli-laser.eu/ for ■.
[5]See https://www.clpu.es/ for ■.
[6]D. Margarone, A. Velyhan, J. Dostal, J. Ullschmied, J. P. Perin, D. Chatain, S. Garcia, P. Bonnay, T. Pisarczyk, R. Dudzak, M. Rosinski, J. Krasa, L. Giuffrida, J. Prokupek, V. Scuderi, J. Psikal, M. Kucharik, M. De Marco, J. Cikhardt, E. Krousky, Z. Kalinowska, T. Chodukowski, G. A. P. Cirrone, and G. Korn, "Proton acceleration driven by a nanosecond laser from a cryogenic thin solid-hydrogen ribbon," Phys. Rev. X 6, 041030 (2016). AQ7
[7]L. Obst, S. Göde, M. Rehwald, F.-E. Brack, J. Branco, S. Bock, M. Bussmann, T. E. Cowan, C. B. Curry, F. Fiuza, M. Gauthier, R. Gebhardt, U. Helbig, A. Huebl, U. Hübner, A. Irman, L. Kazak, J. B. Kim, T. Kluge, S. Kraft, M. Loeser, J. Metzkes, R. Mishra, C. Rödel, H.-P. Schlenvoigt, M. Siebold, J. Tiggesbäumker, S. Wolter, T. Ziegler, U. Schramm, S. H. Glenzer, and K. Zeil, "Efficient laser-driven proton acceleration from cylindrical and planar cryogenic hydrogen jets," Sci. Rep. 10, 1038 (2017).
[8]A. Macchi, M. Borghesi, and M. Passoni, "Ion acceleration by superintense laser-plasma interaction," Rev. Mod. Phys. 85, 751–793 (2013); and references therein.
[9]S. Karsch, S. Düsterer, H. Schwoerer, F. Ewald, D. Habs, M. Hegelich, G. Pretzler, A. Pukhov, K. Witte, and R. Sauerbrey, "High-intensity laser induced ion acceleration from heavy-water droplets," Phys. Rev. Lett. 91, 015001 (2003).
[10]S. Ter-Avetisyan, M. Schnürer, S. Busch, E. Risse, P. V. Nickles, and W. Sandner, "Spectral dips in ion emission emerging from ultrashort laser-driven plasmas," Phys. Rev. Lett. 93, 155006 (2004).
[11]M. Schnurer, S. Ter-Avetisyan, S. Busch, E. Risse, M. P. Kalachnikov, W. Sandner, and P. V. Nickles, "Ion acceleration with ultrafast laser driven water droplets," Laser Part. Beams 23, 337–343 (2005). AQ4
[12]P. Hilz, T. M. Ostermayr, A. Huebl, V. Bagnoud, B. Borm, M. Bussmann, M. Gallei, J. Gebhard, D. Haffa, J. Hartmann, T. Kluge, F. H. Lindner, P. Neumayr, C. G. Schaefer, U. Schramm, P. G. Thirolf, T. F. Rösch, F. Wagner, B. Zielbauer, and J. Schreiber, "Isolated proton bunch acceleration by a petawatt laser pulse," Nat. Commun. ■, ■ (2018). AQ5
[13]P. L. Poole, C. D. Andereck, D. W. Schumacher, R. L. Daskalova, S. Feister, K. M. George, C. Willis, K. U. Akli, and E. A. Chowdhury, "Liquid crystal films as on-demand, variable thickness (50–5000 nm) targets for intense lasers," Phys. Plasmas 21, 063109 (2014).
[14]L. Silva, M. Marti, J. R. Davies, and R. A. Fonseca, "Proton shock acceleration in laser-plasma interactions," Phys. Rev. Lett. 92, 015002 (2004).
[15]E. d'Humières, J. L. Feugeas, P. Nicolaï1, S. Gaillard, T. Cowan, Y. Sentoku, and V. Tikhonchuk, "Investigation of high intensity laser proton acceleration with underdense targets," J. Phys. 244, 042023 (2010).
[16]D. Harberberger, S. Tochitsky, F. Fiuza, C. Gong, R. A. Fonseca, L. O. Silva, W. B. Mori, and C. Joshi, "Collisionless shocks in laser-produced plasma generate monoenergetic high-energy proton beams," Nat. Phys. 8, 95–99 (2012).
[17]C. Palmer, N. P. Dover, I. Pogorelsky, M. Babzien, G. I. Dudnikova, M. Ispiriyan, M. N. Polyanskiy, J. Schreiber, P. Shkolnikov, V. Yakimenko, and Z. Najmudin, "Monoenergetic proton beams accelerated by a radiation pressure driven shock," Phys. Rev. Lett. 106, 014801 (2011).
[18]M. H. Helle, D. F. Gordon, D. Kaganovich, Y. Chen, J. P. Palastro, and A. Ting, "Laser-accelerated ions from a shock-compressed gas foil," Phys. Rev. Lett. 117, 165001 (2016).
[19]F. Sylla, A. Flacco, S. Kahaly, M. Veltcheva, A. Lifschitz, V. Malka, E. d'Humières, I. Andriyash, and V. Tikhonchuk, "Short intense laser pulse collapse in near-critical plasma," Phys. Rev. Lett. 110, 085001 (2013).
[20]S. N. Chen, M. Vranic, T. Gangolf, E. Boella, P. Antici, M. Bailly-Grandvaux, P. Loiseau, H. Pépin, G. Revet, J. J. Santos, A. M. Schroer, M. Starodubtsev, O. Willi, L. O. Silva, E. d'Humières, and J. Fuchs, "Collimated protons accelerated from an overdense gas jet irradiated by a 1 mm wavelength high-intensity short-pulse laser," Sci. Rep. 7, 13505 (2017).
[21]J. L. Henares, T. Tarisien, P. Puyuelo, J.-R. Marquès, T. Nguyen-Bui, F. Gobet, X. Raymond, M. Versteegen, and F. Hannachi, "Optimization of critical-density gas jet targets for laser ion acceleration in the collisionless shockwave acceleration regime," J. Phys. 1079, 012004 (2018).
[22]J. L. Henares, P. Puyuelo-Valdes, F. Hannachi, T. Ceccotti, M. Ehret, F. Gobet, L. Lancia, J.-R. Marquès, J. J. Santos, M. Versteegen, and M. Tarisien, "Development of critical-density gas jet targets for laser-driven ion acceleration," Rev. Sci. Instrum. 90, 063302 (2019).
[23]T. Bonnet, M. Comet, D. Denis-Petit, F. Gobet, F. Hannachi, M. Tarisien, M. Versteegen, and M. M. Aleonard, "Response functions of Fuji imaging plates to monoenergetic protons in the energy range 0.6–3.2 MeV," Rev. Sci. Instrum. 84, 013508 (2013).
[24]See http://www.cenbg.in2p3.fr/-Plateforme-AIFIRA- for ■.
[25]Y. Sentoku and A. J. Kemp, "Numerical methods for particle simulations at extreme densities and temperatures: Weighted particles, relativistic collisions and reduced currents," J. Comput. Phys. 227(14), 6846–6861 (2008).
[26]B. Fryxell, K. Olson, P. Ricker, F. X. Timmes, M. Zingale, D. Q. Lamb, P. MacNeice, R. Rosner, and H. Tufo, "FLASH: An adaptivemesh hydrodynamics code for modelling astrophysical thermonuclearflashes," Astrophys. J. Suppl. Ser. 131, 273–334 (2000).
[27]K. Krushelnick, E. L. Clark, Z. Najmudin, M. Salvati, M. I. K. Santala, M. Tatarakis, and A. E. Dangor, "Multi-MeV ion production from high-intensity laser interactions with underdense plasmas," Phys. Rev. Lett. 83, 737 (1999).
[28]G. S. Sarkisov, V. Y. Bychenkov, V. N. Novikov, V. T. Tikhonchuk, A. Maksimchuk, S.-Y. Chen, R. Wagner, G. Mourou, and D. Umstadter, "Self-focusing, channel formation, and high-energy ion generation in interaction of an intense short laser pulse with a He jet," Phys. Rev. E 59, 7042 (1999).
[29]M. S. Wei, S. P. D. Mangles, Z. Najmudin, B. Walton, A. Gopal, M. Tatarakis, A. E. Dangor, E. L. Clark, R. G. Evans, S. Fritzler, R. J. Clarke, C. Hernandez-Gomez, D. Neely, W. Mori, M. Tzoufras, and K. Krushelnick, "Ion acceleration by collisionless shocks in high-intensity-laser–underdense-plasma interaction," Phys. Rev. Lett. 93, 155003 (2004).

Physics of Plasmas ARTICLE scitation.org/journal/php

[30] L. Willingale, S. P. D. Mangles, P. M. Nilson, R. J. Clarke, A. E. Dangor, M. C. Kaluza, S. Karsch, K. L. Lancaster, W. B. Mori, Z. Najmudin, J. Schreiber, A. G. R. Thomas, M. S. Wei, and K. Krushelnick, "Collimated multi-MeV ion beams from high-intensity laser interactions with underdense plasma," Phys. Rev. Lett. **96**, 245002 (2006).

[31] P. Puyuelo-Valdes, J.-L. Henares, F. Hannachi, T. Ceccotti, J. Domange, M. Ehret, E. D'Humieres, L. Lancia, J.-R. Marquès, J. Santos, and M. Tarisien, "Laser driven ion acceleration in high-density gas jets," Proc. SPIE **11037**, 110370B (2019).

[32] S. C. Wilks, W. L. Kruer, M. Tabak, and A. B. Langdon, "Absorption of ultra-intense laser pulses," Phys. Rev. Lett. **69**, 1383 (1992).

[33] V. Mironov, N. Zharova, E. d'Humìeres, R. Capdessus, and V. T. Tikhonchuk, "Effect of the laser pulse temporal shape on the hole boring efficiency," Plasma Phys. Controlled Fusion **54**, 095008 (2012).

[34] C. S. Brady and T. D. Arber, "An ion acceleration mechanism in laser illuminated targets with internal electron density structure," Plasma Phys. Controlled Fusion **53**, 015001 (2011).

[35] O. Tresca, N. P. Dover, N. Cook, C. Maharjan, M. N. Polyanskiy, Z. Najmudin, P. Shkolnikov, and I. Pogorelsky, "Spectral modification of shock accelerated ions using a hydrodynamically shaped gas target," Phys. Rev. Lett. **115**, 094802 (2015).